


## First-principles study of structural, electronic, elastic, and thermal properties of *Imm*2-BC

Qiang Li(李强), Zhen-Ling Wang(王振玲), Yu-Cheng Yu(于玉城), Lan Ma(马兰), Shao-Li Yang(杨绍利), Hai-Bo Wang(王海波), Rui Zhang(张锐)

**Citation:**Chin. Phys. B . 2019, 28(1): 013101. **doi:** 10.1088/1674-1056/28/1/013101
Journal homepage: http://cpb.iphy.ac.cn; http://iopscience.iop.org/cpb

**What follows is a list of articles you may be interested in**

---

## Density functional theory study of structural stability for gas hydrate

Ping Guo(郭平), Yi-Long Qiu(邱奕龙), Long-Long Li(李龙龙), Qiang Luo(罗强), Jian-Fei Zhao(赵建飞), Yi-Kun Pan(潘意坤)
Chin. Phys. B . 2018, 27(4): 043103. **doi:** 10.1088/1674-1056/27/4/043103

## *Ab-initio* calculations of structural, electronic, and optical properties of $Zn_3(VO_4)_2$

Nisar Ahmed, S Mukhtar, Wei Gao, Syed Zafar Ilyas
Chin. Phys. B . 2018, 27(3): 033101. **doi:** 10.1088/1674-1056/27/3/033101

## CN bond orientation in metal carbonitride endofullerenes:A density functional theory study

Zhu-Xia Zhang(张竹霞), Yong Zhang(张勇), Wen-Hua Xue(薛文华), Wei Jia(贾伟), Cai-Li Zhang(张彩丽), Chun-Xia Li(李春霞), Peng Cui(崔鹏)
Chin. Phys. B . 2017, 26(12): 123102. **doi:** 10.1088/1674-1056/26/12/123102

## Correlation between electronic structure and energy band in Eu-doped $CuInTe_2$ semiconductor compound with chalcopyrite structure

Tai Wang(王泰), Yong-Quan Guo(郭永权), Shuai Li(李帅)
Chin. Phys. B . 2017, 26(10): 103101. **doi:** 10.1088/1674-1056/26/10/103101

## Effect of P impurity on NiAlΣ5 grain boundary from first-principles study

Xue-Lan Hu(胡雪兰), Ruo-Xi Zhao(赵若汐), Yang Luo(罗阳), Qing-Gong Song(宋庆功)
Chin. Phys. B . 2017, 26(2): 023101. **doi:** 10.1088/1674-1056/26/2/023101

---

# First-principles study of structural, electronic, elastic, and thermal properties of *Imm*2-BC*

Qiang Li(李强)[1,†], Zhen-Ling Wang(王振玲)[1], Yu-Cheng Yu(于玉城)[1], Lan Ma(马兰)[1], Shao-Li Yang(杨绍利)[1], Hai-Bo Wang(王海波)[1], and Rui Zhang(张锐)[2]

[1] *College of Vanadium and Titanium, Panzhihua University, Panzhihua* 617000, *China*

[2] *Condensed Matter Science and Technology Institute and Department of Physics, Harbin Institute of Technology, Harbin* 150080, *China*

(Received 28 August 2018; revised manuscript received 17 October 2018; published online 12 December 2018)

Using the first-principles method, we predict an orthorhombic boron–carbon binary structure with space group *Imm*2. This structure is verified to be dynamically and mechanically stable, and possesses a cavity of 27.5 Å$^2$ that makes it a potential molecular sieve material. The C sp$^2$ and sp$^3$ hybridized bonding in *Imm*2 BC is an important factor for its structural stability. The energy band calculations reveal that *Imm*2 BC is a semiconductor with a band gap of 1.3 eV and has a promising application in the electro-optic field. The lattice thermal conductivity along the crystal [100] direction at room temperature is 186 W·m$^{-1}$·K$^{-1}$, that is about 5 times higher than those along the [010] and [001] directions, which stems from the different group velocity along the crystal direction. Moreover, the acoustic-optical coupling is important for heat transport in *Imm*2 BC, and the contribution of optical phonons to lattice thermal conductivity in the [100], [010], and [001] directions is 49%, 59%, and 61%, respectively. This study gives a fundamental understanding of the structural, electronic, elastic, and heat transport properties in *Imm*2 BC, further enriching the family of boron–carbon binary compounds.

**Keywords:** first principles, boron–carbon binary, electronic structure, thermal properties

**PACS:** 31.15.A–, 77.65.–j, 77.84.Cg **DOI:** 10.1088/1674-1056/28/1/013101

## 1. Introduction

Recently, boron–carbon compounds have been widely applied in refractory and shielding material, semiconductor, thermoelectric materials, abrasive powder, and neutron detector due to their high hardness, high melting point, high elastic modulus, low density, and chemical inertness.[1] In recent decades, researchers have investigated various boron–carbon systems using experimental methods.[2–4] It was found that boron–carbon system is a very complicated material that can be identified as rhombohedral phase in the range of 8–20 at.%C. $B_4C$ is the third hardest material in nature and the most widely accepted boron–carbon binary system with space group $R\bar{3}m$. A diamond-like $BC_3$ was synthesized in diamond anvil cell at $2033 \pm 241$ K and 50 GPa.[5] By using a laser-heated diamond anvil cell and large-volume multi-anvil apparatus, a cubic $BC_5$ was successfully synthesized.[6] Theoretically, Saal *et al.*[7] calculated the enthalpy of formation and lattice parameters for boron–carbon systems through the *ab initio* calculations. Their results show that for the carbon-rich 13.33% C composition, the $B_{11}C$-CBC structure is the most stable structure. Using the *ab initio* pseudopotential local orbital approach, Tomanek *et al.*[8] predicted a layered $BC_3$ with graphitic structure. The monolayer of $BC_3$ is a semiconductor, and the metallic energy band of the corresponding bulk structure stems from interactions between the neighboring layers. By performing the particle swarm optimization (PSO) simulations, Luo *et al.*[9] predicted seven stable two-dimension boron–carbon structures ($BC_5$, $BC_3$, $BC_2$, BC, $B_2C$, $B_3C$, and $B_5C$). Li *et al.*[10] performed the first-principles calculations and obtained a hexagonal BC with two atom layers. Through the PSO algorithm and first-principles method, Xu *et al.*[11] predicted two novel structures of $BC_7$ with space groups *Amm*2 and *P*-4*m*2. They claimed that *P*-4*m*2 $BC_7$ is a superhard material. Based on the *ab initio* density functional theory, Hu *et al.*[12] studied seven possible stacking configurations in hexagonal $BC_5$. They proposed that $BC_5$-I with AA stacking sequence is the most stable structure among the seven possible candidates. Although many experimental and theoretical studies have been carried out so far, the bulk boron–carbon binary compounds with an atomic ratio of $B/C = 1$ have not yet been reported in experiments. Thus, this prompts us to search for a potential BC structure with atomic ratio B/C = 1, and then study its electronic structure and thermal properties, which would further enrich the family of bulk boron–carbon binary compounds. The first principles method can predict new materials and their various properties,[13–18] so it is selected for the purpose.

*Project supported by the National Basic Research Program of China (Grant No. 2013CB632900), the Science and Technology Planning Project of Sichuan Province, China (Grant Nos. 2018JY0422 and 2018JY0325), the Department of Education of Sichuan Province, China (Grant No. 18ZA0290), and the Doctor Research Start-up Foundation of Panzhihua University, China (Grant No. 0210600049).

†Corresponding author. E-mail: wslypq@126.com

© 2019 Chinese Physical Society and IOP Publishing Ltd 

## 2. Computational methods and details

Using the QUANTUM-ESPRESSO package[19] with USPEX,[20] we perform first-principles calculations to search for preferable bulk structures of BC. The GBRV pseudopotentials[21] are used to treat the interaction between the electron and nucleus. $2s^2 2p^1$ and $2s^2 2p^2$ configurations are selected to describe the system energy for B and C atoms, respectively. Generalized gradient approximation (GGA) and Perdew–Burke–Ernzerhof (PBE) functional are used to treat the exchange–correlation energy of electrons. A cutoff energy of about 612 eV is adopted to optimize the lattice parameter and relax the atomic positions. The $k$-points spacing of 0.04 $Å^{-1}$ is chosen to sample the Brillouin zone. The convergence of energy is set to $6.8 \times 10^{-7}$ eV/atom. The convergence criteria of forces and lattice stress are set to $1.3 \times 10^{-4}$ eV·$Å^{-1}$ and 0.01 GPa, respectively. The thermal properties are computed using the super-cell method implemented by the phono3py code.[22] The crystal structure and electronic density are depicted by the VESTA.[23] The stress–strain method[24] is applied to calculate the elastic constant.

## 3. Results and discussion

### 3.1. Structure properties

In order to obtain the preferable structures of BC, we build the initial seed structures using the permutation method, then the local structural search is performed by the USPEX.[20] Through further optimizing and symmetrical analysis of the structures obtained from the USPEX, we obtain the final structure with the local minimum energy. This structure belongs to the orthorhombic crystal system with the space group *Imm*2. The atomic coordinates and lattice lattices of *Imm*2 BC that are calculated from the GGA and local-density approximation (LDA) are presented in Table 1 for comparing their differences.

From Table 1, it is found that the lattice parameters show good agreement between the GGA and LDA values and their maximum deviation is smaller than 2%. Thus, the other properties of *Imm*2 BC, e.g., electronic structure and heat transport properties, are calculated by the GGA functional in the next.

The super-cell of *Imm*2 BC is shown in Fig. 1. It can be seen that the predicted *Imm*2 BC has an orthorhombic structure and possesses a cavity of 4.5 Å×6.1 Å (i.e., 27.5 $Å^2$). Thus, *Imm*2 BC would be a potential molecular sieve material. Along the [010] direction, the C1 atom has three nearest neighbors, i.e., two B7 and one C15. The bond length of C1–B7 is about 1.572 Å. The bond length for C1–C15 is 1.376 Å, which is equal to that of 1, 3-butadiene and indicates that the C1–C15 bond is a typical C=C double bond. Compared to the C1 atom, the C3 atom has a different coordination number (4). The bond lengths of C3–B6, B7–C3, and B3–C3 are 1.591 Å, 1.585 Å, and 1.563 Å, respectively. Their maximum difference is only 0.028 Å, which implies that the C1 atom locates in a tetrahedron of B and has a $sp^3$ hybridization bonding with four B atoms. Each B atom has three nearest neighbor C along the [001] and [010] directions. The calculated bond lengths are 1.572 Å, 1.584 Å, 1.563 Å, and 1.591 Å for the B7–C1, B7–C3, C6–B6, and B6–C3 atom pairs, respectively. The angles of C3–B7–C1, C3–B7–C1, C6–B6–C6, and C6–B6–C3 are 120.9°, 118.0°, 119.1°, and 120.3°, respectively. This suggests that the B atoms occur $sp^2$ hybridization and have covalent bonding with the around C atoms. Next, the electronic localization function is calculated to well illustrate this problem.

**Table 1.** Calculated lattice parameters $a$, $b$, and $c$ with different exchange correlation functionals for *Imm*2 BC.

| | Lattice constant/Å | | Deviation/% |
|---|---|---|---|
| | LDA | GGA | |
| $a$ | 2.6696 | 2.6954 | 0.96 |
| $b$ | 13.6300 | 13.8546 | 1.62 |
| $c$ | 4.4239 | 4.4624 | 0.86 |
| | Atomic coordinate | | Deviation/% |
| B1(4$d$) | 0.0000 | 0.0000 | 0.00 |
| | 0.8913 | 0.8923 | 0.11 |
| | 0.4050 | 0.4009 | 1.02 |
| B2(4$d$) | 0.0000 | 0.0000 | 0.00 |
| | 0.7430 | 0.7427 | 0.04 |
| | 0.6644 | 0.6702 | 0.87 |
| C1(4$d$) | 0.0000 | 0.0000 | 0.00 |
| | 0.5500 | 0.5497 | 0.05 |
| | 0.9292 | 0.9211 | 0.88 |
| C2(4$d$) | 0.0000 | 0.0000 | 0.00 |
| | 0.2208 | 0.2200 | 0.36 |
| | 0.3268 | 0.3331 | 1.89 |

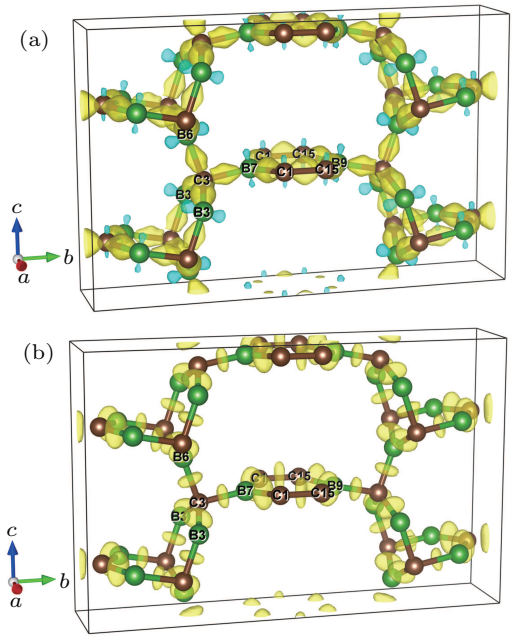



**Fig. 1.** The predicted crystal structure: (a) electronic localization function and (b) difference charge density for *Imm*2 BC. Brown spheres are C cations, and green ones are B cations.

The B atom usually exhibits a $sp^2$ bonding with the others in its compounds,[25] and C usually shows two bond types, e.g., $sp^2$ in graphite and $sp^3$ in diamond. In this work, the obtained *Imm*2 BC per formula unit has seven valence electrons, which could form a stable orthorhombic structure. This is very different from the case of bulk BN that has eight electrons per formula unit. Therefore, the bonding analysis is helpful for understanding the electronic characteristic of the orthorhombic BC. The electronic localization function (ELF) is considered an important tool for studying the lone pair electrons and bonding electrons, and can be written as[26]

$$\eta(r) = \frac{1}{[1+\chi^2_{\mathrm{BE}}(r)]}, \tag{1}$$

where $\chi_{\mathrm{BE}}(r) = D(r)/D_{\mathrm{h}}(r)$, $D_{\mathrm{h}}(r) = 3/5(6\pi^2)^{2/3}\rho(r)^{5/3}$, and $\rho$ is the electron density.

The volume ELF distribution of *Imm*2 BC is shown in Fig. 1(a). It is observed that the localized electron density appears between the C6–B6, B6–C3, C3–B3, C3–B7, B7–C1, C1–C15, and C15–B9 atom pairs, which suggests that the covalent bonding occurs between these atoms. This conclusion is in good agreement with the analysis of bond length and bond angle above.

We also investigate the different charge density to analyze the electronic properties of *Imm*2 BC as shown in Fig. 1(b). We find that the $p_z$ electrons transfer from the B7, C1, C15, B9, B3, and B6 atoms to the bonding region of the B–C (and C–C) bonds, suggesting that these atoms occur $sp^2$ hybridization, while the C6 and C3 atoms exhibit obvious $sp^3$ hybridization. From the above analysis on the ELF and different charge density, we can know that two different orbital hybridizations of C appear in *Imm*2 BC, and they are the important factor for the structure stability.

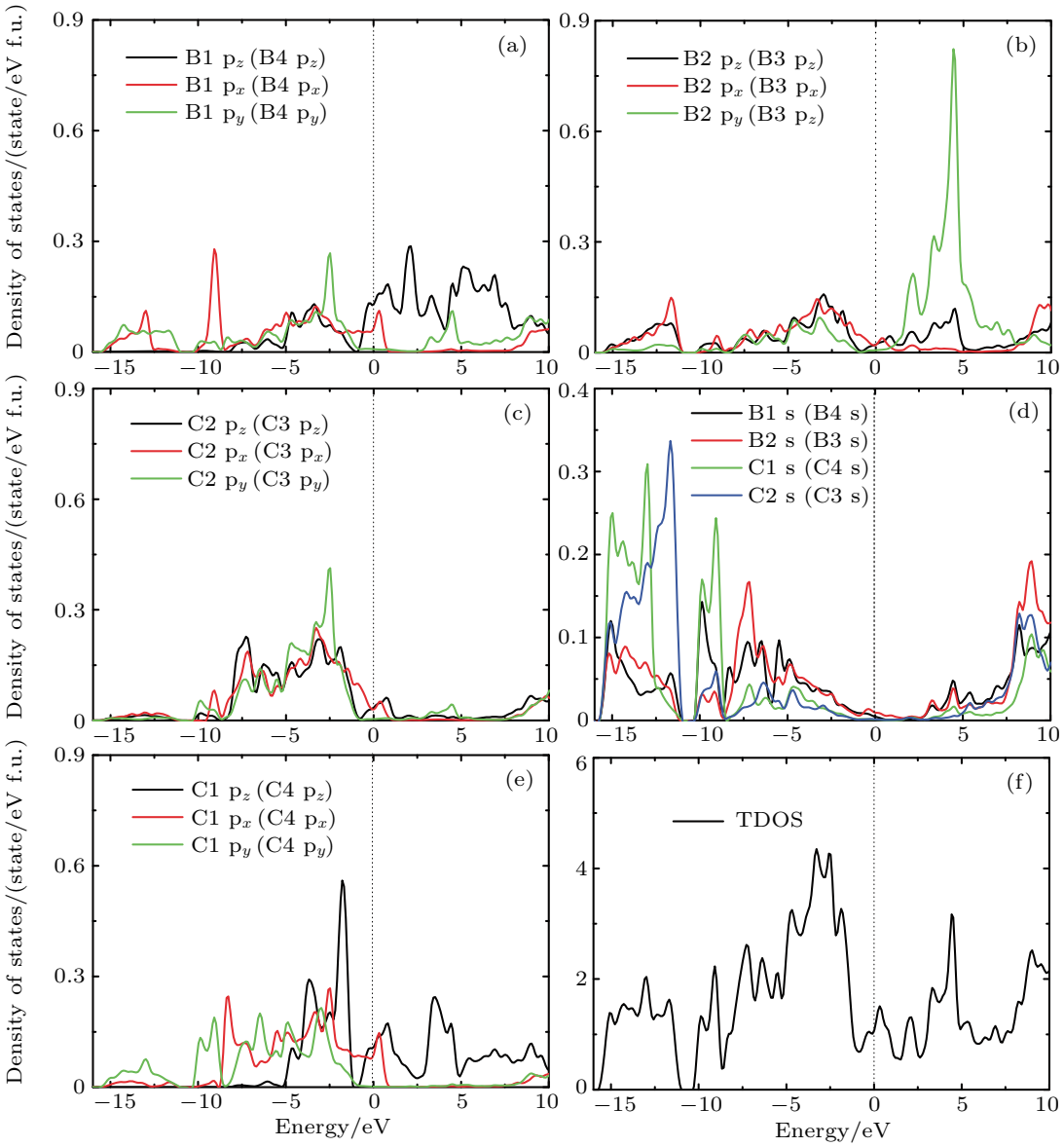



**Fig. 2.** The calculated (f) total and (a)–(e) partial density of states for *Imm*2 BC with a primitive cell that includes four B (B1, B2, B3, and B4) and four C (C1, C2, C3, and C4) atoms.

In order to understand the electronic properties of *Imm*2 BC, we calculate its total and partial density of states (DOS) at zero pressure as shown in Fig. 2. It is found that both the C1 and C4 (or both the C2 and C3) atoms are in the same atomic environment, leading to the same electronic states. This also applies to the B1 and B4 atoms as well as B2 and B3 atoms. As shown in Fig. 2, the valence band (VB) is dominated by the C1 and C2 s states mixing a few B1 and B2 s states in the energy range from −16.0 eV to −11.0 eV, suggesting that there exists covalent bonding between the C and B atoms. The s, $p_x$, and $p_y$ states of the B1 and C1 atoms resonate in the range from −16 eV to 10 eV, indicating that they occur $sp^2$ hybridization in this region. The energy states at the top of VB consist of the C1 and C4 $p_z$ states which can be assigned to C=C double bonds. The C2 $p_x$ and $p_y$ states are almost identical with the $p_z$ state, illustrating that the C2 atom occurs $sp^3$ hybridization. The B2 $p_z$ state is almost the same as the $p_x$ state, and its $p_y$ state shows the unoccupied case. This implies that the B2 atom occurs $sp^2$ hybridization. Moreover, there are some energy states around the Fermi level, which indicates that *Imm*2 BC may be a half-metal.

The projected energy band is believed to be a useful tool to analyze the energy states, thus we plot the atomic projected energy band in Fig. 3 to clarify whether *Imm*2 BC is a half-metal. From Fig. 3, we see that the C and B $p_x$ states cross the Fermi level, then form the unoccupied states in the *W*–*X* direction. The C and B $p_z$ states cross the Fermi level, resulting in that the occupied energy bands appear in the *W*–*X* direction.

Although the B and C $p_x$ states overlap with their $p_z$ states as shown in Fig. 3, the electron transition between the $p_x$ and $p_z$ states is symmetry forbidden. Therefore, *Imm*2 BC is a semiconductor and the calculated band gap is 1.3 eV. Because the B and C atoms form the covalent bonds and their $p_z$ states have the same symmetry that fulfills the transition rule, the electron transition would occur between the C and B $p_z$ bonding states and antibonding states at the *S* (or *W*) point in the Brillouin zone.

Figure 4(a) presents the simulated x-ray diffraction (XRD) spectra (using copper radiation). It is clear that *Imm*2 BC has three peaks at about 13°, 21°, and 26°. It can be seen from Fig. 4(b) that there are three Raman peaks at 20.6 THz, 30.2 THz, and 34.5 THz, respectively. The Raman peaks (33.1 $cm^{-1}$ and 34.5 $cm^{-1}$) are too close to be distinguished. The simulated XRD and Raman spectra can be used as the reference for experiments.

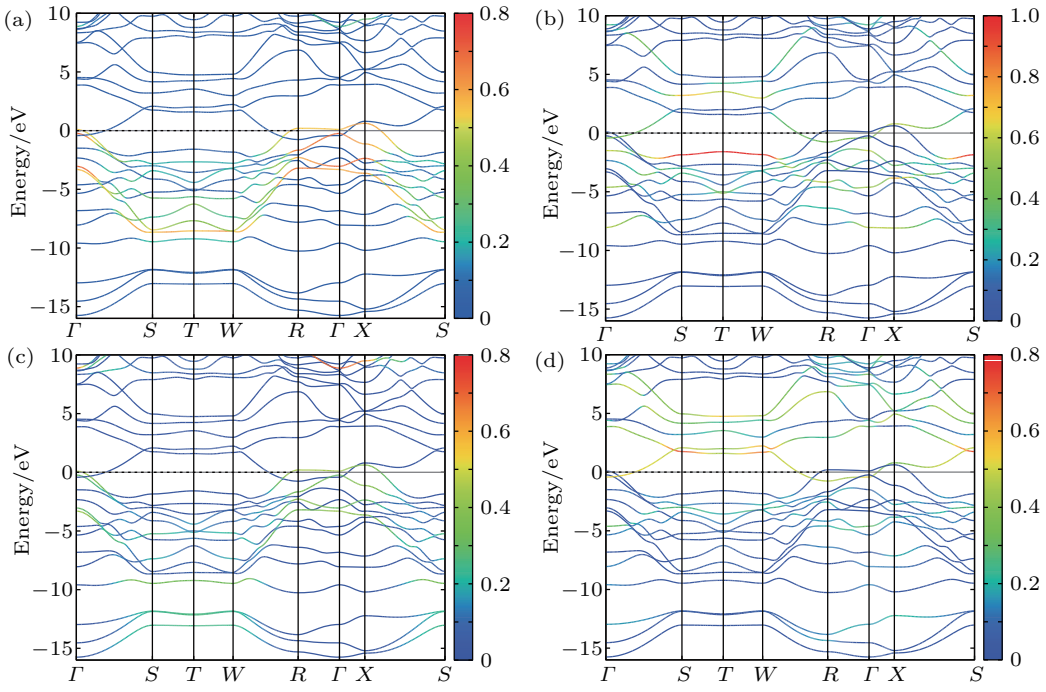



**Fig. 3.** The calculated projected energy bands with (a) C $p_x$, (b) C $p_z$, (c) B $p_x$, and (d) B $p_z$ states for *Imm*2 BC.

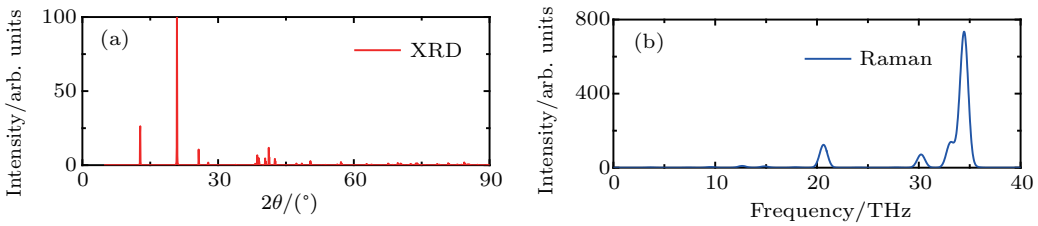



**Fig. 4.** Simulated (a) XRD and (b) Raman spectra for *Imm*2 BC.

### 3.2. Elastic properties

In order to confirm the mechanical stability of *Imm*2 BC, we calculate its elastic constant with a $6\times6$ symmetric matrix as follows:

$$\boldsymbol{c}=\begin{pmatrix} 537.97 & 073.72 & 62.58 & 0 & 0 & 0 \\ 73.72 & 201.77 & 94.16 & 0 & 0 & 0 \\ 62.58 & 94.16 & 135.68 & 0 & 0 & 0 \\ 0 & 0 & 0 & 8.81 & 0 & 0 \\ 0 & 0 & 0 & 0 & 71.57 & 0 \\ 0 & 0 & 0 & 0 & 0 & 137.41 \end{pmatrix}. \quad (2)$$

For an orthorhombic crystal, the generalized elastic stability criteria[27] are given by

$$c_{ii}>0, \quad (i=1,2,\ldots,6), \quad (3)$$

$$M_1=(c_{11}+c_{33}-2c_{13})>0, \quad (4)$$

$$M_2=[c_{11}+c_{22}+c_{33}+2(c_{12}+c_{13}+c_{23})]>0, \quad (5)$$

$$M_3=(c_{11}+c_{22}-2c_{12})>0, \quad (6)$$

$$M_4=(c_{22}+c_{33}-2c_{23})>0. \quad (7)$$

One can see that the calculated $c_{11}$, $c_{22}$, $c_{33}$, $c_{44}$, $c_{55}$, and $c_{66}$ are greater than zero, which meets the elastic stability criteria $c_{ii}>0$. The other criteria are $M_1=584$ GPa, $M_2=1336$ GPa, $M_3=666$ GPa, and $M_4=243$ GPa, and they are also greater than zero, which satisfies the elastic stability criteria given by Eqs. (4)–(7). Therefore, *Imm*2 BC is mechanically stable under the ambient condition.

For *Imm*2 BC, there are nine independent elastic constants as shown in Eq. (2). From the calculated elastic constants $c_{ij}$, some mechanical parameters of *Imm*2 BC, e.g., bulk modulus ($B$) and shear modulus ($G$), can be calculated through Voigt–Reuss–Hill (VRH) approximation.[28] The VRH $B_{\rm H}$ is defined as the average $B_{\rm H}=(B_{\rm V}+B_{\rm R})/2$ between the Voigt $B_{\rm V}$ and Reuss $B_{\rm R}$, where

$$B_{\rm V}=\frac{1}{9}(c_{11}+c_{22}+c_{33})+\frac{2}{9}(c_{12}+c_{13}+c_{23}), \quad (8)$$

$$B_{\rm R}=\frac{1}{(s_{11}+s_{22}+s_{33})+2(s_{12}+s_{13}+s_{23})}. \quad (9)$$

The VRH $G_{\rm H}=(G_{\rm V}+G_{\rm R})/2$ is the average between the Voigt upper $G_{\rm V}$ and Reuss $G_{\rm R}$, where

$$G_{\rm V}=\frac{1}{15}(c_{11}+c_{22}+c_{33}-c_{12}-c_{13}-c_{23})+\frac{1}{5}(c_{44}+c_{55}+c_{66}), \quad (10)$$

$$G_{\rm R}=\frac{15}{4(s_{11}+s_{22}+s_{33})-4(s_{12}+s_{13}+s_{23})+3(s_{44}+s_{55}+s_{66})}. \quad (11)$$

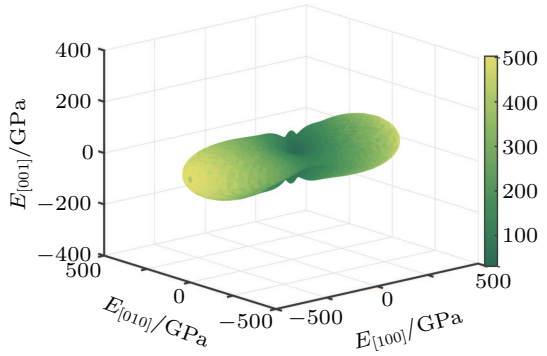



**Fig. 5.** (color online) The calculated Young's modulus for *Imm*2 BC.

The calculated $B_{\rm H}$ and $G_{\rm H}$ for *Imm*2 BC are 133 GPa and 57 GPa, respectively. The $B_{\rm H}/G_{\rm H}$ ratio is usually used to distinguish the brittleness or ductility of materials. The $B_{\rm H}/G_{\rm H}$ ratio has a value larger than 1.75, suggesting that this material is ductile. Conversely, it is brittle. The obtained $B_{\rm H}/G_{\rm H}$ ratio of *Imm*2 BC is 2.33 (larger than 1.75), which indicates that *Imm*2 BC is brittle. $B_{\rm H}$, $G_{\rm H}$, and $B_{\rm H}/G_{\rm H}$ are suitable for describing polycrystalline systems, while Young's modulus ($E$) can be used to estimate the elastic anisotropy of single crystal materials.[29] As shown in Fig. 5, the calculated $E$ of *Imm*2 BC along the [100] direction is 502 GPa at zero pressure, considerably larger than the values (134 GPa and 90) along the [010] and [001] directions, which indicates that *Imm*2 BC shows a strong elastic anisotropy.

### 3.3. Phonon properties

The calculated phonon dispersion and phonon partial densities of states are presented in Fig. 6, in which no imaginary phonon modes are found, confirming the dynamical stability of *Imm*2 BC. The B atoms are mainly responsible for the frequency vibrations in the range of 9–21 THz, and the C atoms contribute to the low frequency parts in the range of 2–9 THz. The maximum frequency peak at 42.3 THz is predominantly from the C=C stretching vibration. Moreover, the acoustic-optical frequency gap is not found in the phonon dispersion, and the significant acoustic-optical coupling in *Imm*2 BC is observed in the range of 5–15 THz. Thus, the lattice thermal conductivity of *Imm*2 BC contains some contribution from the optical modes. The dynamical stability of *Imm*2 BC is also examined by first-principles molecular dynamics simulations with a 1 fs time step. *Imm*2 BC is structurally complete when the temperature is below 850 K, and the break of the B–C bonds is observed when the temperature is higher than 870 K. Thus *Imm*2 BC is structurally stable between 300 K and 850 K.

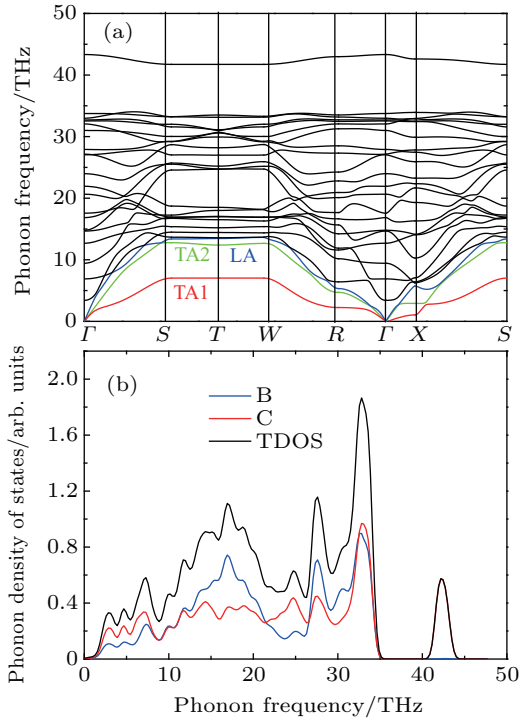



**Fig. 6.** The predicted (a) phonon dispersion and (b) phonon partial density of states for *Imm*2 BC.

### 3.4. Lattice thermal conductivity

The lattice thermal conductivity (LTC) is calculated by the following equation:[22]

$$\kappa = \frac{1}{NV_0}\sum_{\lambda} C_\lambda \nu_\lambda \otimes \nu_\lambda \tau_\lambda, \tag{12}$$

where $V_0$ is the volume of the unit cell, $C_\lambda$ is the mode dependent heat capacity, $\boldsymbol{\nu}_\lambda$ is the phonon group velocity, and $\tau_\lambda$ is the phonon lifetime. Based on the second and third order interatomic force constants obtained from the super-cell method, the LTC of *Imm*2 BC along the $x$, $y$, and $z$ directions (i.e., [100], [010], and [001] directions) are calculated as shown in Fig. 7. To understand features of the intrinsic LTC of *Imm*2 BC, the other contributions (e.g., boundary scattering) are not included in the present work.

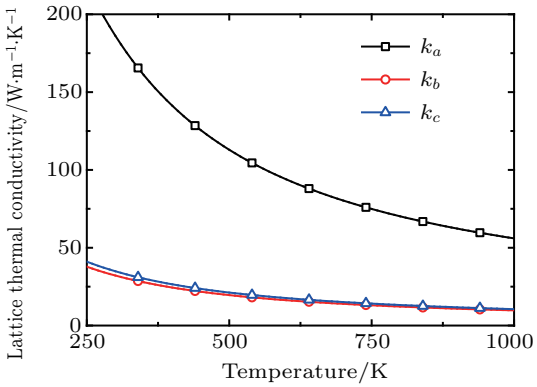



**Fig. 7.** The calculated lattice thermal conductivity for *Imm*2 BC using first-principles method.

From Fig. 7, it is found that at 300 K, the $k_b$ and $k_c$ of *Imm*2 BC have an almost equal value (i.e., 31 W·m$^{-1}$·K$^{-1}$ and 34 W·m$^{-1}$·K$^{-1}$), suggesting that *Imm*2 BC has almost the same atomic distribution along the [010] and [001] directions. Along the [100] direction, the $k_a$ at room temperature is 186 W·m$^{-1}$·K$^{-1}$, which is about 5 times higher than that along the [010] and [001] directions; this indicates that the LTC of *Imm*2 BC is anisotropic. To illustrate the LTC anisotropy in *Imm*2 BC, we calculate the average outer product of group velocity $\nu \otimes \nu$ along the [100], [010], and [001] directions. The $\nu \otimes \nu$ in the [100] direction is 25169 THz$^2$·Å$^2$, which is about 5 times higher than that (i.e., 4360 THz$^2$·Å$^2$ and 5296 THz$^2$·Å$^2$) in the [010] and [001] directions, suggesting that the LTC anisotropy in *Imm*2 BC is caused by the different group velocity along the crystal direction.

In order to understand the relationship between the thermal conductivity and phonon lifetime of *Imm*2 BC, we calculate the phonon lifetime $\tau$ by the first-principles super-cell method, and the results are shown in Fig. 8. It is found that the integral $\tau$ at 300 K is about 100 ps, and then decreases to 44 ps when the temperature increases to 600 K. When the temperature increases to 1000 K, the integral $\tau$ decreases to 25 ps, which is about 3 times smaller than that at 300 K. Through Eq. (12), it is well known that the $k$ is proportional to the phonon lifetime $\tau$. The average $k$ of 84 W·m$^{-1}$·K$^{-1}$ at 300 K is about 3 times that at 1000 K, thus the decrease in phonon lifetime with the temperature is the major cause of the decrease of LTC. Moreover, it is found that the phonon lifetime in the region of 0–7.5 THz mainly comes from the contribution of three acoustic modes, and the other region is dominated by the optical modes. This indicates that the LTC might be from the contribution of both the acoustic and optical modes.

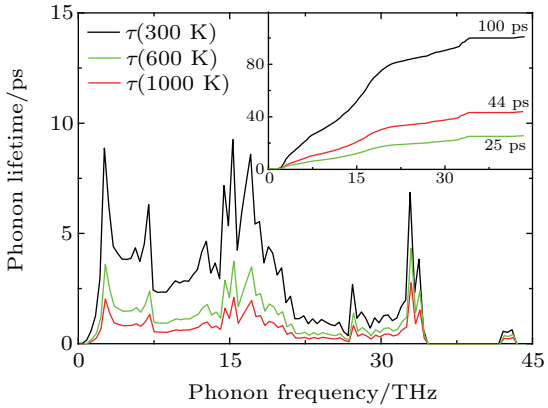



**Fig. 8.** The calculated phonon lifetime as a function of phonon frequency for *Imm*2 BC. Integral phonon lifetime is shown in the inset.

In order to verify the preliminary inspection above, we calculate the LTC of *Imm*2 BC with respect to the phonon branch as shown in Fig. 9. It is found that the maximum LTC contribution in the [100] direction comes from the contribution of the first phonon mode (23%), while the largest LTC along the [010] direction is derived from the second phonon mode (30%). These two maximum LTCs originate from the

contribution of acoustic modes in common. The largest LTC in [001] direction stems from the fifth phonon mode, i.e., the optical mode, and the corresponding contribution is up to 22%. This is obviously different from the case in both the [100] and [010] directions. The calculated contribution of optical phonons to LTC along the [100], [010], and [001] directions are 49%, 59%, and 61%, respectively, suggesting that the acoustic-optical coupling is important for phonon transport in *Imm*2 BC.

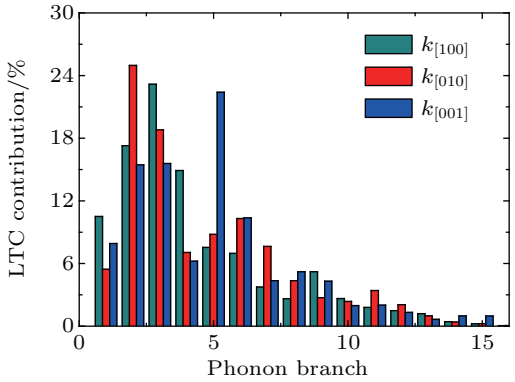



**Fig. 9.** The contribution to lattice thermal conductivity from phonon branches of *Imm*2 BC at 300 K.

## 4. Conclusion

In this work, the first-principles method successfully predicts a bulk boron–carbon binary system with space group *Imm*2. The elastic constant and phonon spectra calculations suggest that this structure is dynamically and mechanically stable. The C $sp^2$ and $sp^3$ hybridized bonding in *Imm*2 BC is the important factor for its structural stability. The analysis of structure indicates that *Imm*2 BC is a potential molecular sieve material. The energy band calculations illustrate that *Imm*2 BC is a semiconductor with a band gap of 1.3 eV and has a promising application in the optoelectronic field. The lattice thermal conductivity in the [100] direction is 186 $W{\cdot}m^{-1}{\cdot}K^{-1}$, around 5 times higher than that in the [010] and [001] directions, which shows that the lattice thermal conductivity of *Imm*2 BC is anisotropic, and the reason can be ascribed to the different group velocity along the crystal direction. Moreover, the contribution of optical phonons to lattice thermal conductivity in the [100], [010], and [001] directions is 49%, 59%, and 61%, respectively. Thus, the acoustic-optical coupling is important for heat transport in *Imm*2 BC. Moreover, the simulated XRD and Raman spectra can be used as the reference for experiments.

## References


[1] Suri A K, Subramanian C, Sonber J K and Murthy T S R C 2010 *Int. Mater. Rev.* **55** 4
[2] Emin D 2006 *J. Solid State Chem.* **179** 2791
[3] Bouchacourt M and Thevenot F 1981 *J. Less-Common Met* **82** 227
[4] Bouchacourt M and Thevenot F 1979 *J. Less-Common Met* **67** 327
[5] Zinin P V, Ming L C, Kudryashov I, Konishi N and Sharma S K 2007 *J. Raman Spectrosc.* **38** 1362
[6] Solozhenko V L, Kurakevych O O, Andrault D, Godec Y L and Mezouar M 2009 *Phys. Rev. Lett.* **102** 015506
[7] Saal J E, Shang S and Liu Z K 2007 *Appl. Phys. Lett.* **91** 231915
[8] Tomanek D, Wentzcovitch R M, Louie S G and Cohen M L 1988 *Phys. Rev. B* **37** 3134
[9] Luo X, Yang J, Liu H, Wu X, Wang Y, Ma Y, Wei S H, Gong X and Xiang H 2011 *J. Am. Chem. Soc.* **133** 16285
[10] Li Q, Zhang R, Lv T and He Z 2016 *Ceram Int.* **42** 4026
[11] Xu L, Zhao Z, Wang Q, Wang L-M, Xu B, He J and Tian Y 2011 *J. Appl. Phys.* **110** 013501
[12] Hu Q, Wu Q, Ma Y, Zhang L, Liu Z, He J, Sun H, Wang H T and Tian Y 2006 *Phys. Rev. B* **73** 214116
[13] Li Q, Rui Z, Lv T Q and Zheng L M 2015 *Chin. Phys. B* **24** 053101
[14] Li Q, Zhang R and Lv T 2017 *Comp Mater. Sci.* **128** 22
[15] Qi Y M, Chen H L, Jin P, Lu H Y and Cui C X 2018 *Acta Phys. Sin.* **67** 067101 (in Chinese)
[16] Zhang Z, Wang H, Wang K Y, An H, Liu B, Wu J C and Zou Y 2018 *Acta Phys. Sin.* **67** 046101 (in Chinese)
[17] Cheng W, Fu Y L, Ying M J and Zhang F S 2017 *Chin. Phys. Lett.* **34** 127101
[18] Shi J, Gao Y, Wang X L and Yun S N 2017 *Chin. Phys. Lett.* **34** 087701
[19] Giannozzi P 2009 *J. Phys: Condens Matter* **21** 395502
[20] Lyakhov A O, Oganov A R, Stokes H T and Zhu Q 2013 *Comput. Phys. Commun.* **184** 1172
[21] Garrity K F, Bennett J W, Rabe K M and Vanderbilt D 2014 *Comp Mater. Sci.* **81** 446
[22] Togo A, Chaput L and Tanaka I 2015 *Phys. Rev. B* **91** 094306
[23] Momma K and Izumi F 2011 *J. Appl. Crystallogr.* **44** 1272
[24] Yu R, Zhu J and Ye H Q 2010 *Comput. Phys. Commun.* **181** 671
[25] Teii K, Ito H, Katayama N and Matsumoto S 2015 *J. Appl. Phys.* **117** 055710
[26] Becke A D and Edgecombe K E 1990 *J. Chem. Phys.* **92** 5397
[27] Piskunov S, Heifets E, Eglitis R I and Borstel G 2004 *Comp Mater. Sci.* **29** 165
[28] Hill R 1963 *J. Mech. Phys. Solids* **11** 357
[29] Bachmann F, Hielscher R and Schaeben H 2010 *Solid State Phenom.* **160** 63